2023

Spatiotemporal analysis of extreme precipitation in the Southern Great Plains hydroclimate region

P. Flanagan

R. Mahmood
University of Nebraska - Lincoln

Spatiotemporal Analysis of Extreme Precipitation in the Southern Great Plains Hydroclimate Region

PAUL XAVIER FLANAGAN[a] AND REZAUL MAHMOOD[b,c]

[a] *Agricultural Research Service, U.S. Department of Agriculture, El Reno, Oklahoma*
[b] *High Plains Regional Climate Center, Lincoln, Nebraska*
[c] *School of Natural Resources, University of Nebraska–Lincoln, Lincoln, Nebraska*

(Manuscript received 18 April 2022, in final form 19 December 2022)

ABSTRACT: The southern Great Plains (SGP) is defined by hydrometeorological swings between dry and wet extremes. These swings exacerbate the climatological gradients of moisture (from east to west) and temperature (from south to north), which can impact the agricultural production of the region. Thus, it is key to understand extremes to sustainably maintain agricultural success in the region. This study investigates the wet extremes, or extreme precipitation events, that have become more prominent in the last two decades. Data from 108 U.S. Historical Climatology Network stations were analyzed for the 1950–2020 period to detect changes in the frequency and magnitude of extreme precipitation events. Results show that changes in the magnitude of extreme precipitation are isolated and scattered across the SGP, with only the winter season showing regional shifts in extreme precipitation magnitude. Changes in the frequency of extreme precipitation events were noted across the entire SGP, although the changes in frequency are more notable in the eastern SGP than in the western SGP. Analysis shows that the increased number of events detected is driven more, but not exclusively, by the increasing spatial extent of individual extreme precipitation events than by an increased number of events. Overall, these results depict the changing nature of extreme precipitation within the SGP and differences in extreme precipitation between the eastern and western SGP.

KEYWORDS: Extreme events; Precipitation; Trends

1. Introduction

The Great Plains (GP) region of the United States is defined by two different climatological gradients: the west-to-east increase of precipitation and the north-to-south increase in temperature (Borchert 1950; Christian et al. 2015; Flanagan et al. 2017; Qiao et al. 2017; Tollerud et al. 2018; Adhikari et al. 2019; Mullens and McPherson 2019). These gradients create a special hydroclimatic pattern across the GP, where seasonally, regions of the GP do not receive enough precipitation relative to evaporation (Seager et al. 2018; Adhikari et al. 2019; Adhikari and Hansen 2019). This is especially true in the southern GP (SGP) where the western SGP receives significantly less precipitation than is lost to evapotranspiration during the summer. Even so, agriculture and livestock production are common across the western region. Further, the warmth of the SGP, as compared with the northern GP (NGP), creates a very different hydroclimate regime. In the NGP, soil moisture recharges earlier in the winter period prior to the soil freezing, relative to the SGP where the soil moisture state is closely tied to draw down from plant transpiration during the late spring and summer and recharge during the late autumn, winter, and early spring (Illston et al. 2004). This creates two different springtime hydroclimate regimes, where in the NGP the springtime thaw can introduce large amounts of water to the hydrological system, which, along with extreme precipitation can lead to very large floods, such as the historic flood of 2019 (Flanagan et al. 2020). In the SGP, the lack of a true thaw in the spring does not create this situation and thus river flooding due to excessive water is more dependent on excessive precipitation over time rather than one extreme precipitation event, such as in the May 2015 flooding of Oklahoma and Texas in the Red River watershed (Simon Wang et al. 2015; Wugofski 2019).

Beyond the hydroclimatic perspective, extreme precipitation also has large implications for agriculture and livestock. While large-scale floods are not as common in the SGP as in the NGP, flash floods can still lead to widespread damages in a region, especially to agriculture and the ecosystem (Michaud et al. 2001; Westra et al. 2014; Mallakpour and Villarini 2015; Mullens 2021). Flash floods can cause large amounts of soil disturbance and riverbank erosion that permanently alters the ecosystem and landscape. While agricultural fields are not as susceptible to impactful erosion like grazing lands if managed properly (Joyce et al. 2001; Thornes 2007; Papanastasis 2009), removal of topsoil through heavy precipitation is still a real threat to agricultural lands especially during fallow periods (Pimentel et al. 1987; Montgomery 2007). Large amounts of precipitation with copious runoff can impact agriculture by disturbing the soil at varying times during the growing season, including planting, seeding, and fallow periods in which the soils and crops are at particularly delicate stages in their life cycles (Neild 1982; Urban et al. 2015; Mäkinen et al. 2018; Liu and Basso 2020). In addition, timing of fertilizer and irrigation use is critical as an extreme precipitation event immediately after fertilization and irrigation could yield damage to the ecosystem or excessive runoff and possible erosion damage to the agricultural land (Patrignani et al. 2014; Ghimire et al. 2018). The result of this is the infiltration of pollutants into river

Corresponding author: Paul Flanagan, paul.flanagan2@usda.gov

DOI: 10.1175/JAMC-D-22-0071.1

systems after heavy precipitation events. This leaking of pollutants can damage the river ecosystem of the region, with greater impacts from this contaminated runoff after heavier precipitation events or floods (Sharpley et al. 1987; Rosenberg and Smith 2009). Thus, improved knowledge of the climate of extreme precipitation in the SGP is necessary for the development of conservation or best management practices to foster sustainable agricultural practices within the region.

Given the importance of the SGP in terms of agricultural production in the United States, the region has been a focus for hydroclimate research, especially related to the region's extremes. The Fourth National Climate Assessment (NCA4) noted the changes in precipitation across the SGP and found that the amount of precipitation in the heaviest events, or magnitude of extreme precipitation, has been increasing, even as overall precipitation appears to be declining in the region (Hayhoe et al. 2018). They also found that precipitation extremes were projected to increase in the SGP in all CMIP5 emission scenarios and locally constructed analogs (LOCA) downscaled climate model analyses. To that end, many studies on SGP extreme precipitation focus on the analysis of future precipitation extremes. Janssen et al. (2014) analyzed U.S. Cooperative Observer Network station data and CMIP5 model data to find that extreme precipitation is increasing over portions of the United States, including the SGP. Kunkel et al. (1999) also analyzed station data across the United States for trends within extreme precipitation frequency and found that areas from the southwestern United States across the Great Plains and into the midwestern United States showed positive and statistically significant trends in the occurrence of 7-day 1-yr return period precipitation events for the 1931–96 period.

These results are not unique and many studies (e.g., Kunkel et al. 1999; Min et al. 2011; Higgins and Kousky 2013; Mullens et al. 2013; Feng et al. 2016; Easterling et al. 2017; Bartels et al. 2020; Kunkel et al. 2020; Davenport et al. 2021; Moustakis et al. 2021), with varying degrees of certainty, show that extreme precipitation is increasing across the GP, including the SGP. The causes of these increases are varied and include links to increased atmospheric moisture through either climate change or changes in the GP low-level jet (GPLLJ; Min et al. 2011; Feng et al. 2016; Kunkel et al. 2020; Davenport et al. 2021), internal climate variability (Kunkel et al. 1999; Higgins and Kousky 2013), and changes in convective storms in conjunction with either of the previous causes (Feng et al. 2016; Easterling et al. 2017; Moustakis et al. 2021). It is likely that the drivers of the increases in extreme precipitation are seasonally linked, rather than a single persistent annual driver (Ruiz-Barradas and Nigam 2010; Mullens et al. 2013; Davenport et al. 2021) and thus necessitating a seasonal analysis of extreme precipitation at fine scales. Further, the hydroclimate of the SGP is driven by a variety of phenomena, primarily through the GPLLJ (e.g., Helfand and Schubert 1995; Higgins et al. 1997a; Ting and Wang 1997; Ruiz-Barradas and Nigam 2005; Berg et al. 2015), organized convection (Fritsch et al. 1986; Wang et al. 2013; Feng et al. 2016; Haberlie and Ashley 2019; Hu et al. 2021), and the dryline (Hoch and Markowski 2005; Mitchell and Schultz 2020). Given that these factors work at different times of the year, a seasonal analysis will provide more information on the impact of each factor on extreme precipitation trends.

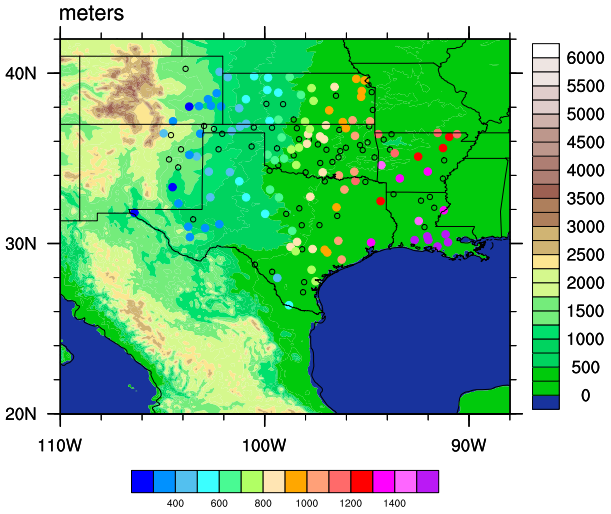

FIG. 1. Map of the study area. The color-filled circles represent stations used within the study, and the open circles represent stations that were excluded by the 10%-or-more-missing-data filter. The background map color fill is terrain height (m). The color fill in each circle is the annual precipitation climatology (mm) for the USHCN stations over the SGP.

Although previous research has investigated extreme precipitation in the SGP, many of these studies have not focused on the station-level changes to extreme precipitation but rather on a regionally or climate division averaged view of extreme precipitation (e.g., Kunkel et al. 1999; Min et al. 2011; Higgins and Kousky 2013; Easterling et al. 2017; Bartels et al. 2020; Kunkel et al. 2020; Davenport et al. 2021; Moustakis et al. 2021). The objective of this research was to break down those coarser area average views into the station-level assessment and to provide in-depth statistics for extreme precipitation climatology and any trends associated with this climatology in the SGP region. A secondary objective is to identify linkages between these statistics, spatially and temporally, with previously investigated causes of the trends in extreme precipitation frequency and magnitude within the SGP. The results from this research will improve our understanding of trends in the frequency and magnitude of extreme precipitation in the SGP at the station or local level, which will also aid in establishing the links between these trends and extremes and the causes of the enhanced precipitation in the study area.

2. Data and methods

a. Station data criteria

We have used data from the stations located within Colorado, New Mexico, Kansas, Oklahoma, Texas, Arkansas, and Louisiana (Fig. 1). Because there is no single dominant watershed within this region, several watersheds were of focus, including but not limited to the Red River, the Colorado River, and the Arkansas River. Given the influence of terrain on extreme precipitation, stations west of 105°W within

Colorado and New Mexico were not used. Further, stations east of 91°W were removed to provide focus on the southern plains and Gulf Coastal plains region, hereinafter defined as the SGP in this work. The region was defined in a way so that we could include observations from watersheds that would provide a complete understanding of extreme precipitation within this hydroclimatic region. Given the different climates of the western and eastern SGP, stations were split along the 100°W longitude to define the eastern SGP (east of 100°W) and western SGP (west of 100°W).

U.S. Historical Climatology Network (USHCN; Menne et al. 2012) daily, version 3, data were chosen because of their long period of record, quality, and spatial density of observations. A total of 108 stations (of 171 total SGP USHCN stations) were selected with data from 1 January 1950 to 31 December 2020, with a maximum of 10% missing observations (Fig. 1). Note that increasing the missing data requirement to 20% only added 7 stations to the analysis and thus did not increase the number of stations significantly. Although the number of stations is unequal between the two subregions, analysis of extreme precipitation completed shows that both regions are distinctly different with regard to extreme precipitation and thus warrant the additional separate analyses. One caveat of note for this study is the definition of a day within this particular dataset. Numerous data sources are contained within the USHCN-Daily dataset, with the most prominent being from the NWS's Cooperative Observer Program (COOP). The COOP daily summaries are considered to be primary sources of observational data for the USHCN-Daily dataset being created using manual observations, and thus numerous stations with the USHCN-Daily dataset are from the COOP network, given that they pass the period of record and quality checks mentioned in Menne et al. (2012). However, using the COOP network means that the 24-h period over which observations are taken for a "daily" summary is dependent on when the observations are taken at each station. Thus, the 24-h daily precipitation observations may represent different 24-h periods when compared with one another. However, the USHCN dataset addressed this "time of observation bias" issue and mitigated it as much as they could (Durre et al. 2010; Menne et al. 2012). Given that time of observation is not recorded within the USHCN-Daily dataset, it is not possible to determine from which 24-h periods each daily precipitation measurement is taken. Nonetheless, while these (and more) caveats and biases are known to exist within the USHCN dataset, this time series is composed of the longest and most consistently recorded observations.

b. *Extreme event definition*

The methodology used in this study is the same as that used in Flanagan and Mahmood (2021) in which extreme precipitation events are defined using the top 1% (99th percentile) of all events and by the annual station maximum precipitation (highest precipitation amount recorded by each station during the year) amount. Further, this definition was extended to all stations and per station. The "all station" extreme definition uses all precipitation days (precipitation $\geq$ 0.0 mm) from all stations and hence, a regionwide climatology providing a single threshold from precipitating days from a time series composed of all precipitation events from all stations throughout the 1950–2020 period. The "per station" extreme precipitation climatology considered each station separately, thus calculating a separate threshold from all precipitation days at each station. This was used to provide a local analysis of each station and to identify local changes in the magnitude of extreme precipitation. Because daily totals were used in this analysis, it is possible that a multiday extreme precipitation event occurred across the boundary of 2–3 days and thus not be identified as an extreme event. Because of this, an analysis measuring the 99th-percentile threshold and annual maximum threshold trends in 3-day sums of precipitation was completed. These results showed similar results to what was found when daily totals were used to identify extreme precipitation events and thus our analysis focused on the extreme precipitation events identified using 1-day totals. In addition, it should be mentioned that all methods used to define precipitation thresholds in this study did not include no-precipitation (0.0 mm) days.

Because of the seasonality in precipitation within the SGP (Mock 1996; Livneh and Hoerling 2016; Flanagan et al. 2017, 2018) the analysis was broken down into seasons including winter [December–February (DJF)], spring [March–May (MAM)], summer [June–August (JJA)], and autumn [September–November (SON)]. A shifted definition of seasons was also used in which winter is defined as January–March (JFM), spring is April–June (AMJ), summer is July–September (JAS), and autumn is October–December (OND). This definition is more attuned to the timing of the GPLLJ, which is vitally important to the precipitation of the SGP (Song et al. 2005; Ruiz-Barradas and Nigam 2005, 2006; Cook et al. 2008; Weaver and Nigam 2008). Frozen precipitation is recorded as its water equivalent in the USHCN time series. Thus, a separate analysis of frozen precipitation, such as snow, hail, or freezing rain, was not included in this study. Due to stations near the Gulf of Mexico being included in this analysis, an assessment was done by removing tropical cyclone (TC) events to determine if they had an impact on the results. To complete this, landfalling TC events were removed from the analysis along with the top 10 precipitation-producing TC events for Texas, Oklahoma, and Louisiana to eliminate the impact of inland precipitation from post landfalling TC events. This analysis showed that either including or removing TC events produced very similar results. The primary difference between the two is that a few stations either lost statistical significance or gained statistical significance across the entire domain. Thus, our analysis includes TC events within the extreme precipitation dataset.

Analogous to Flanagan and Mahmood (2021), the temporal increase or decrease, that is, trends in extreme precipitation frequency (counts) and magnitude (annual maximum or 99th percentile) were calculated using a Theil–Sen's trend estimator built into the National Center for Atmospheric Research (NCAR) Command Language (NCL; https://doi.org/10.5065/D6WD3XH5). Given the large range of extreme precipitation values, a method insensitive to outliers to calculate these trends was necessary. Theil–Sen's trend estimations are insensitive to

outliers and thus is significantly more accurate than simple linear regressions (Wilcox 1999). Trends using Theil–Sen's estimation method are calculated by fitting a line through all pairs of points in the dataset and then determining the median of the slopes of those lines. Mann–Kendall was used along with the Theil–Sen's trend estimator to test for significance (p value of 0.05 or the 95th-percent significance level) of the calculated trends. The Mann–Kendall test is a rank-based, nonparametric statistical test that compares the differences in signs between earlier and later data points to detect any trends within the chronological data (Mann 1945; Kendall 1975). Using this methodology, annual trends were estimated using a time series of annual maximum events or events that surpassed the 99th-percentile threshold. Seasonal trends were estimated in the same fashion, but from the time series computed from each 3-month period.

To rule out the impact of autocorrelation within each station's precipitation time series, autocorrelations were calculated and tested against two-tailed confidence intervals using an N of 108. Any time series with significant autocorrelations were tapered with a split-cosine-bell tapering (prewhitening) using a prebuilt NCL command (taper) on 10% of the station's time series. Comparison between these results and those without tapering showed little difference, and thus the tapered time series were used for the analysis.

Similar to Flanagan and Mahmood (2021) and as used in Howarth et al. (2019), two different methods were used to objectively count extreme precipitation events. This was done to analyze trends and changes in the frequency of extreme precipitation in the SGP. The set thresholds were used to analyze the frequency of events near the all-station 99th-percentile threshold (75 mm) and approximately 50 mm (i.e., 125 mm) and 100 mm (i.e., 175 mm) above the 75-mm threshold. We adopted this approach because of the wide range of 99th-percentiles across the SGP region. Thus, setting a threshold near the regionwide 99th percentile would depict the regional differences in the eastern and western SGP. Included was a unique event method and every event method. In the unique event method only a single event that crosses the three thresholds (75, 125, and 175 mm) was counted for any day. Once a single event was detected at any station, the method would move to the next day and start again. Thus, this gives a count of extreme precipitation events that is disconnected from their spatial patterns and is more focused on the frequency of the events. The second method counted every single event that crossed any of the three thresholds across the entire domain. Thus, multiple precipitation events could be counted for any day. When the trends are compared between the two methods, changes in the spatial extent of extreme precipitation events in the SGP can be examined. If the trend in the number of unique events is not increasing in frequency but the count of every event is increasing, or the trend using the count of every event is increasing at a larger rate than the unique event trend, then it is likely that the spatial extent of the extreme events is increasing rather than the frequency alone. The unique event method ignores the impact of multiple extreme precipitation events (different precipitation events in different regions of the SGP) on the same day. Thus, it is not possible to account for multiple unique extreme precipitation events on a given day within the unique event methodology. Still, comparing the extreme precipitation event counts calculated from all events crossing the various thresholds (every event) and the method counting only a singular event each day that crosses the threshold (unique event) provides an understanding of the change in the spatial extent of extreme precipitation in the SGP. Trends were calculated across the entire time series, with mean number of events per year being calculated through each half of the time series with a prior to 1984 and after 1984. Other split points were tested (i.e., 1970 and 1995), but results were nearly identical to the 1984 split point.

3. Results

a. SGP precipitation climatology

It is well known that annual precipitation in the SGP decreases from east to west, from over 1500 mm yr^{-1} in the far eastern SGP to around 200–300 mm in the far western SGP (Borchert 1950; Christian et al. 2015; Mullens and McPherson 2019; Fig. 1). This decrease of precipitation is also associated with a decrease in frequency and magnitude of extreme precipitation events (Fig. 2a). The number of all-station 99th percentile precipitation events decrease from around 150–200 events over the 70-yr (1950–2020) period in the southeastern SGP (Louisiana) to less than 25 in the western SGP (Fig. 2a). The magnitude of these extreme precipitation events also changes from east to west (Fig. 2a). However, this change is different from the frequency, as larger station maximum precipitation events occur in the central SGP (Fig. 3a). Station maximum precipitation events above 300 mm occur primarily along the Louisiana and Texas coastline. Events of this large magnitude are also found inland and thus are likely not associated with landfalling tropical cyclones but can also be connected to convective activity prevalent within the SGP (Doswell et al. 1996; Schumacher and Johnson 2005; Haberlie and Ashley 2019) or large-scale systems such as post landfall tropical cyclones. Across most of the central and western SGP, the isolated nature (large-magnitude events not surrounded by similar magnitude observations) of the station maximum events from around 100–200 mm seems affiliated with isolated or organized convection.

This is summarized in Fig. 2a, which shows each precipitation amount greater than 99th percentile, using the all-station 99th-percentile threshold (73.7 mm). Stations west of 100°W have far fewer 99th-percentile precipitation events relative to the eastern SGP when the same threshold is used for all stations. These results hold even if a 99th-percentile threshold using only stations from their respective region, that is, the eastern and western SGP (Fig. 2b), is computed. Although the number of events in the western SGP increases relative to the eastern SGP, the overall number of events per station is still larger in the eastern SGP than in the western SGP. Further, the 99th-percentile threshold decreases from 78.0 mm in the eastern SGP to 50.8 mm in the western SGP. Given these results, separate climates of extreme precipitation exist across the SGP. The much larger frequency of extreme precipitation events in the eastern SGP cannot be explained solely by landfalling tropical systems as they only occur in the later portion

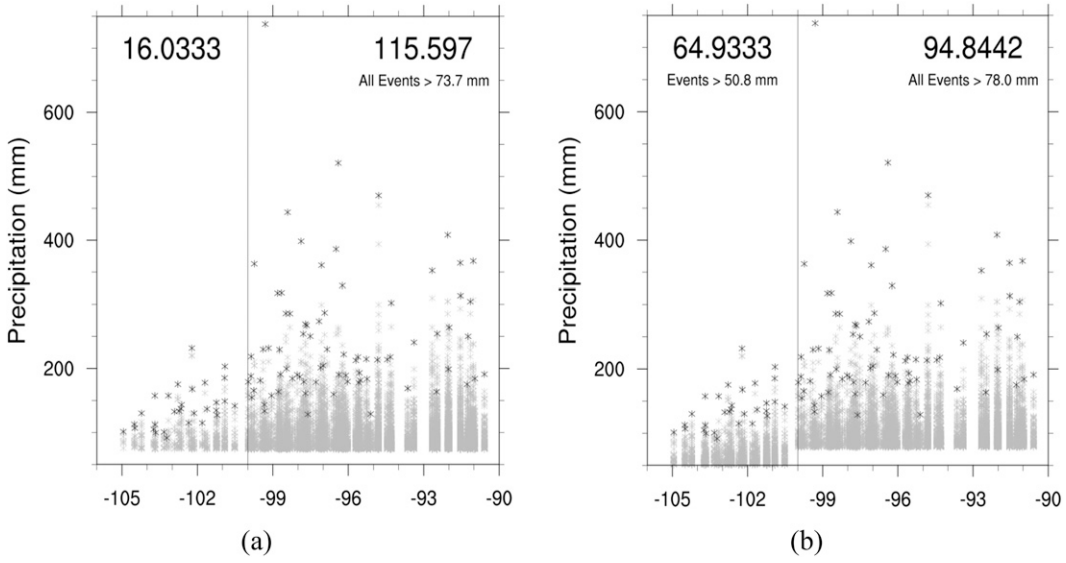

FIG. 2. The magnitude (mm) of each (a) above-all-station-99th-percentile-threshold precipitation event and (b) above-99th-percentile-threshold precipitation event defined using only western (left side of each plot) and eastern (right side of each plot) SGP stations for the 1950–2020 period. Large-font values at the top represent the number of events per station for the 71-yr period, and small-font values represent the value of the 99th-percentile threshold used for those stations. Black data points represent the station maximum precipitation event that occurred for that station across the 1950–2020 period. Stations are ordered by their longitudinal position from west (left-hand side) to east (right-hand side). The solid line at −100° longitude value separates the eastern and western SGP stations values.

of the year and do not occur frequently, with only a few a year at most (Lyons 2004; Doyle 2009). A driver of heavy precipitation in the eastern SGP is organized convection, such as mesoscale convective systems (MCSs), which can produce excessive precipitation amounts across wide areas. These occur mainly in the eastern GP (within both the NGP and SGP) and thus would solely increase the frequency of extreme precipitation events in the eastern SGP.

The seasonal analysis of station maximum precipitation events further displays the differences between the western and eastern SGP. Large-magnitude (≥125 mm) station maximum precipitation events are concentrated in MAM, JJA, and SON (Texas mainly) west of 100°W, while east of 100°W large-magnitude events appear across all four seasons especially near the Texas and Louisiana coastlines. During SON (Fig. 3b) and DJF (Fig. 3c), most station maximum precipitation events west of 100°W are less than 100 mm (all stations in DJF, 23/31 stations in SON) with few stations seeing events around 150–250 mm (8 of 31 stations in SON). During MAM (Fig. 3d) and JJA (Fig. 3e), stations west of 100°W observe larger station maximum events above 100 mm with more of the stations going over 150- or 200-mm events (12 of 31 in MAM and 22 of 31 in JJA) in comparison with SON and DJF. In the eastern SGP, greater than 150 mm station maximum events are found across all four seasons. Closer to the coastline, the station maximum events are very large, with >200-mm precipitation events during all four seasons. In the central SGP, season maximum events are larger during the convectively active portions of the year (MAM, JJA, and SON) with widespread larger-magnitude events in JJA and SON. This result is likely linked, again, to organized convection such as MCSs that tend to occur predominantly during this time of year (Fritsch et al. 1986; Wang et al. 2013; Feng et al. 2016; Haberlie and Ashley 2019; Hu et al. 2021) and or tropical cyclone events during the late summer and early autumn seasons.

b. *Annual and seasonal extreme precipitation trends*

1) STATION MAXIMUM PRECIPITATION TRENDS

Analysis of annual station maximum precipitation trends (Fig. 4a) show a spatially scattered pattern of statistically significant increasing trends across the SGP. Only a single statistically significant negative trend is seen in the far western portion of the study domain. The predominant signal in statistically significant trends is increasing in station maximum annual events. Two distinct areas of statistical significance are observed, one across the coastal areas of eastern Texas and Louisiana and the other in the spring and summer convective regions of the central and northern SGP. The statistically significant coastal trends are above >0.5 mm yr^{-1} in magnitude, while the central and northern SGP significant trends range from 0.0 to 0.1 mm yr^{-1} to >0.5 mm yr^{-1} magnitude. The noncoastal larger-magnitude statistically significant increasing trends are primarily located within Oklahoma and Kansas, although the localized nature of convection during spring and summer could mask trends in these small-scale storms in the less dense observation network in western and central Texas.

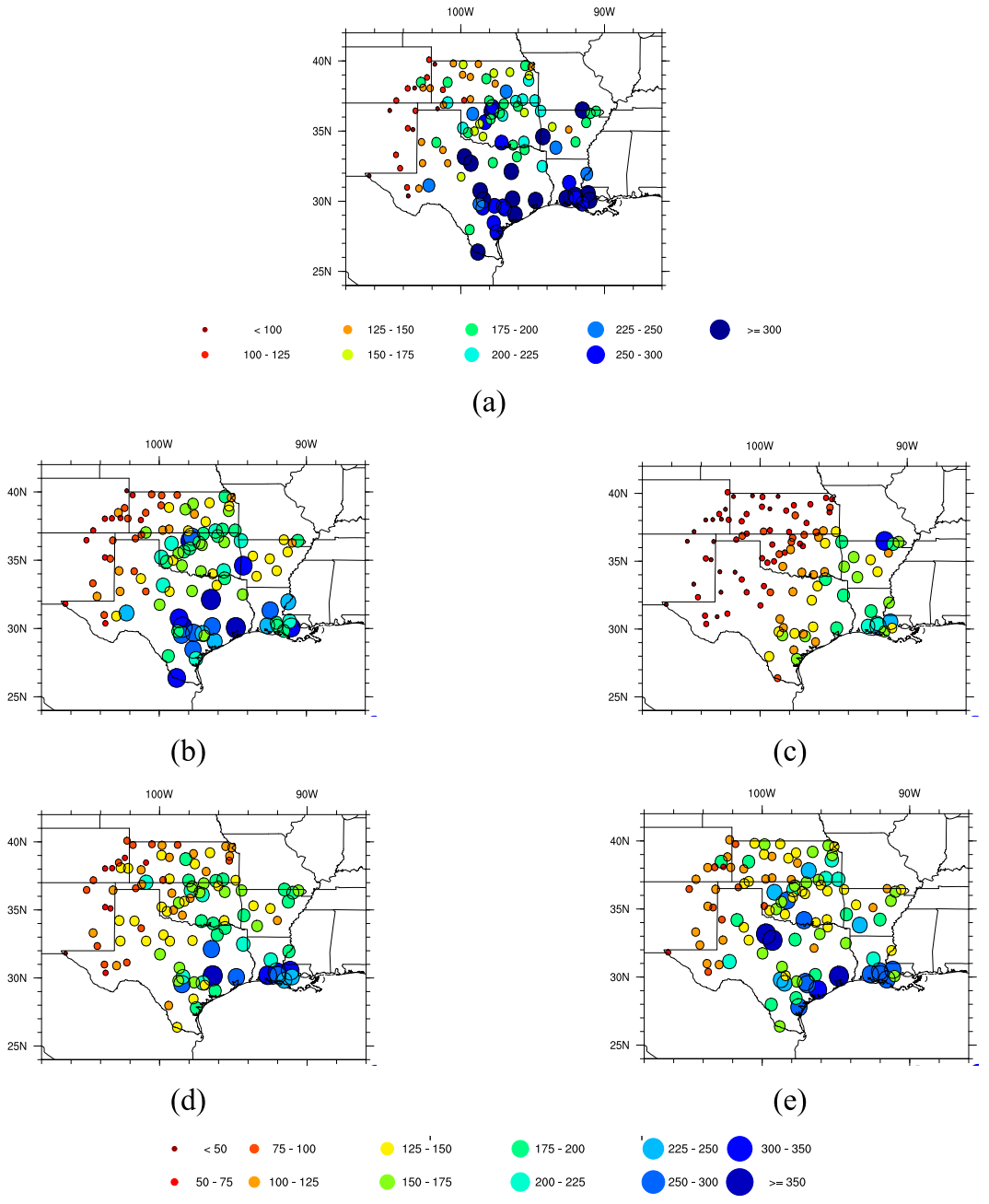

FIG. 3. Station daily maximum precipitation amount (mm) between 1950 and 2020 for (a) annual, (b) SON, (c) DJF, (d) MAM, and (e) JJA.

Seasonally, the station maximum analysis shows a few different trends across the four 3-month periods analyzed. Outside of the DJF period, statistically significant trends are very isolated and scattered across the SGP, like the annual station maximum precipitation trends (Fig. 4a). In SON (Fig. 4b), statistically significant increasing trends are very scattered across the entire inland portion of the domain, with larger-magnitude (>0.5 mm yr^{-1}) trends located across the Gulf of Mexico coastline. DJF (Fig. 4c) shows widespread statistically significant increasing trends across the northern and central portions of the study area (Kansas, Oklahoma, and northwestern Texas). MAM (Fig. 4d) and JJA (Fig. 4e) trends are generally like the annual (Fig. 4a) station maximum trends. In MAM, the statistically significant trends are primarily in the central portion of the domain, along the Kansas and Oklahoma borders. In JJA, the statistically significant trends are scattered across the inland portion of the SGP, with a more concentrated region of statistically significant increasing trends seen in eastern Colorado.

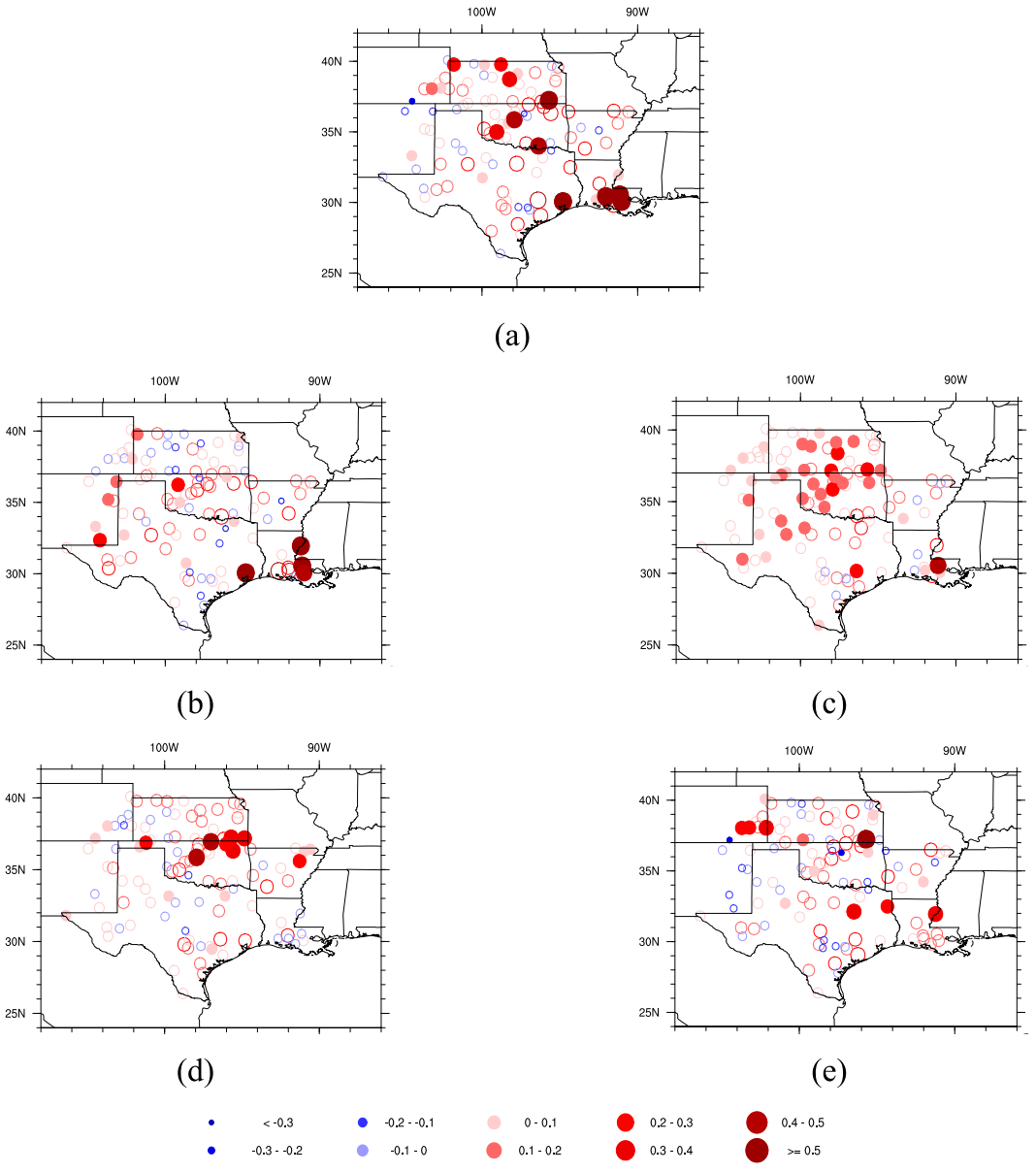

FIG. 4. Regression slope analysis of annual maximum daily precipitation event by station for (a) annual, (b) SON, (c) DJF, (d) MAM, and (e) JJA. The size of the circle and its color denote the magnitude (larger circles denote increased magnitudes) determined through a Theil–Sen trend estimation method, with the filled circles showing a statistically significant trend determined with a Mann–Kendall trend significance test. Prewhitening was completed on any station with a statistically significant autocorrelation (two-tailed t test with an N of 108). Units are in millimeters per year, with significance measured at the 95% significance level (p value of 0.05).

2) 99TH-PERCENTILE PRECIPITATION THRESHOLD TRENDS

Like the annual station maximum trends, the 99th-percentile trends (Fig. 5a) depict scattered and increasing statistically significant trends across the SGP. However, the large-magnitude (>0.5 mm yr^{-1}) statistically significant trends along the coastline are not evident within the 99th-percentile trend analysis. Statistically significant trends are found in Louisiana and eastern Texas near the coastline, but the stations are fewer and the trends are lower in magnitude relative to the station maximum trends (Fig. 4a). Further, while the statistical significance is more consistent within the convectively active region of the northern and central SGP, the trends are not as large in magnitude relative to the annual station maximum trends, with no statistically significant trend found over the 0.4–0.5 mm yr^{-1} range.

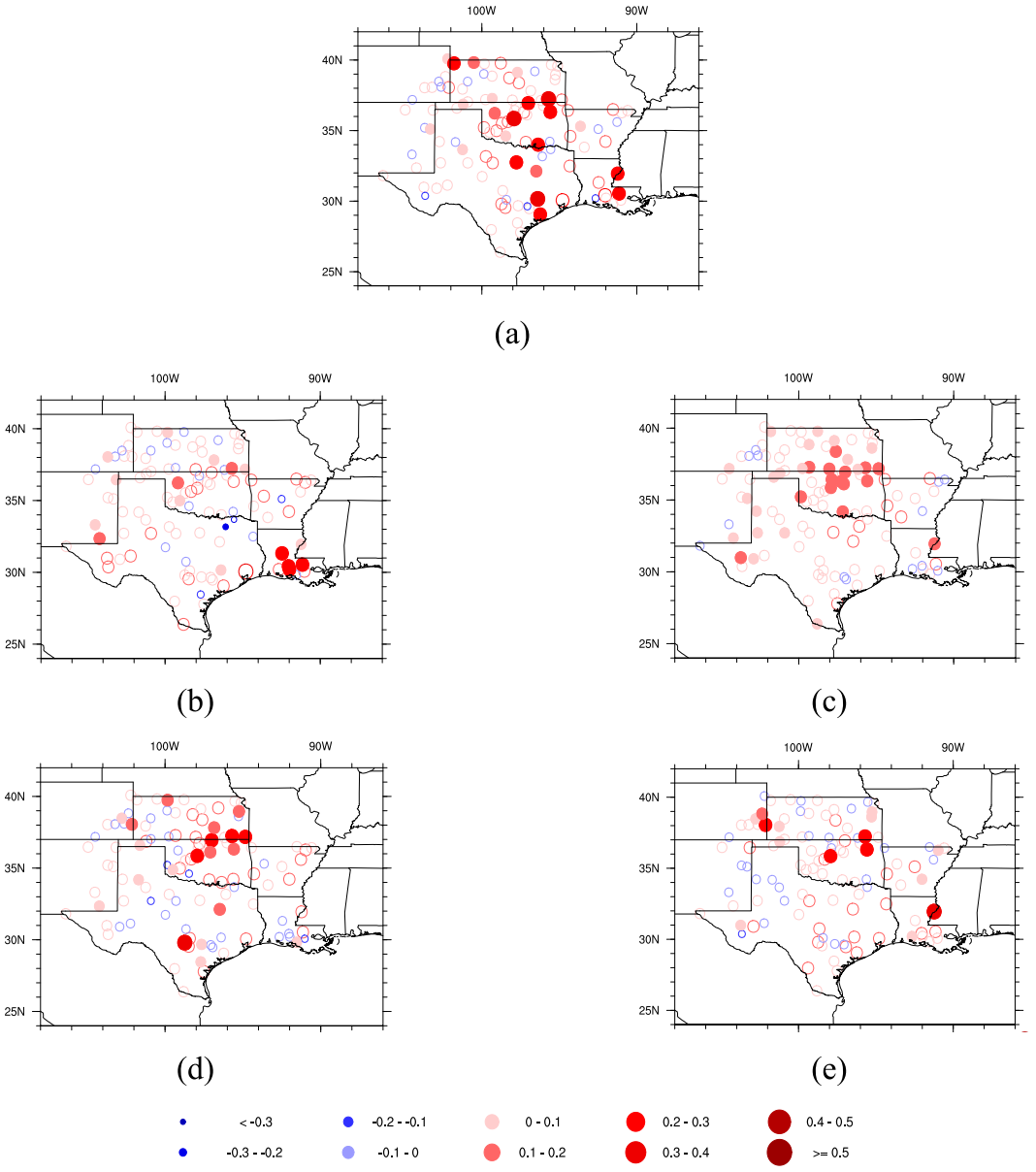

FIG. 5. As in Fig. 4, but for the 99th-percentile threshold.

Seasonally, outside of the DJF trends, the statistically significant 99th-percentile trends are very isolated and scattered across the SGP. The statistically significant increasing trends do not go over the 0.5 mm yr^{-1} in magnitude, with a majority of the significant trends being in the 0.0–0.2 mm yr^{-1} range. SON (Fig. 5b) 99th-percentile trends show several statistically significant increasing trends along the Gulf of Mexico coastline, which is not seen in the annual 99th-percentile trend analysis. The DJF (Fig. 5c), MAM (Fig. 5d), and JJA (Fig. 5e) 99th-percentile statistically significant trends depict nearly identical features as those found in the station maximum analysis, however, with reduced magnitudes. DJF trends show widespread statistically significant increasing trends in the northern and central portion of the study domain. MAM and JJA trends are less consistent, with MAM showing a region of statistically significant increasing trends along the Kansas and Oklahoma border, whereas JJA statistically significant trends are spatially very scattered.

c. *Extreme precipitation event frequency*

1) SGP EXTREME PRECIPITATION EVENT COUNT

The purpose of the analysis of the extreme precipitation event counts, through counting using the unique event or the all-event method, was to achieve a measure of change in frequency and the spatial extent of the extreme precipitation events in the SGP. While both the unique and all-event methodologies provide an understanding of the change in frequency of events, comparisons of the unique and all-event counts can assist in identifying the

change in spatial extent of such events. If events are increasing at a higher rate (larger trend) in the all-event count than in the unique event count, then it stands to reason that the spatial extent of the extreme events is increasing. For the SGP unique event counts (Figs. 6a,c,e), the number of extreme events (≥75, 125, and 175 mm) are larger across the 1984 time boundary, and thus it appears that extreme precipitation events are increasing in frequency across this region. However, the all-event counts (Figs. 6b,d,f) show a statistically significant increasing trend (shown in Fig. 6 below each panel's letter) that is larger in magnitude (3 times as large) in comparison with the unique event counts. When considering percent change (calculated as the difference in means between the two periods divided by the earlier period mean) within each figure, the change within the unique event counts is larger when considering the 125- and 175-mm analyses. Owing to the statistical significance of trends in both the unique and all-event counts for the 75-, 125-, and 175-mm-threshold analyses, changes in both the frequency and spatial extent of extreme precipitation events can be inferred from these results.

2) SUBREGIONAL EXTREME PRECIPITATION EVENTS

Given the difference in the two SGP subregions, the extreme precipitation event counts were also divided into eastern (Figs. 7a,c) and western SGP (Figs. 7b,d) analyses. As indicated previously, the number of stations is greater in the eastern SGP than in the western SGP, and this distribution could impact their comparisons. To address this issue, counts were completed by randomly selecting 25 (25 of 77 for the eastern SGP and 25 of 31 in the western SGP) stations from each region (not shown). Analysis of data from these 25 stations shows that the eastern SGP had more ≥75-mm extreme precipitation events (mid-20s per year) than did the western SGP (~3 per year). Thus, it appears that the number of stations is not impacting the analysis of extreme precipitation events counts and the following analysis was created using all stations in the eastern and western SGP.

In the eastern SGP (Figs. 7a,c), the distribution of events through the all-event and unique event counts is like the frequency analysis completed on the entire SGP region. The unique event counts (Fig. 7a) depict a small increasing trend (0.138 events per year) across the 71-yr period. The all-event counts (Fig. 7c) show a larger increasing trend (0.348 events per year), again identifying the importance of the increased spatial extent of extreme precipitation events in the eastern SGP within the analysis of >75-mm extreme precipitation events. However, in the western SGP (Figs. 7b,d) the results are different. For the lowest extreme precipitation threshold analyzed, the number of unique and all-events ≥75-mm precipitation appears to be decreasing in the western SGP (Figs. 7b,d), but the Mann–Kendall slope analysis depicts a 0.0 trend for both the unique and all-event counts in the western SGP.

3) SEASONAL DISTRIBUTION OF EXTREME PRECIPITATION EVENTS

The seasonal distribution of precipitation in the SGP is bimodal with a peak in the late spring–early summer period and a second peak during the early-autumn period (Malinowski et al. 2007; Flanagan et al. 2017). The distribution of extreme precipitation events (≥73.7 mm or the all-station 99th percentile; Fig. 8) follows this climatological pattern, with more events in the spring, summer, and autumn seasons than in the winter season in both the western and eastern SGP (Fig. 8a). This is more evident in the shifted seasonal analysis, which was designed to match more with the climatology of the GPLLJ. The AMJ, JAS, and OND 3-month periods (Fig. 8b) show many more extreme precipitation events in both the eastern and western SGP when compared with the JFM 3-month period. Even though lower in comparison with SON, extreme precipitation events do occur in OND in the eastern SGP with increased frequency relative to the JFM period. As such, it appears that extreme precipitation in the eastern SGP occurs year-round, although at a much-reduced rate during DJFM, whereas the western SGP rarely has any extreme precipitation events during the DJFM period.

4. Discussion

Although the drivers of the identified trends cannot be directly investigated using only precipitation data, inferences can be made given the spatial patterns of the statistical changes. Precipitation in the SGP is seasonally dependent (Flanagan et al. 2017), but results show that extreme precipitation occurs at all times of the year, at least in the eastern SGP. While MAM, JJA, and SON extreme precipitation events can be linked to convection and convective systems such as MCSs (Fritsch et al. 1986; Wang et al. 2013; Feng et al. 2016; Haberlie and Ashley 2019; Hu et al. 2021), DJF extreme precipitation events are more than likely linked to anomalously strong synoptic waves (Deng and Jiang 2011; Grise et al. 2013). Thus, the casual mechanisms driving the increased magnitude of extreme precipitation during DJF are different when compared with MAM, JJA, and SON. While changes in GP extreme precipitation events during MAM, JJA, and SON are likely linked to anomalies in the GPLLJ, DJF extreme events occur independent of the GPLLJ and thus are likely related to changes in synoptic wave characteristics or mean temperature changes.

Starting in the winter (DJF), analysis shows widespread central GP (Oklahoma, Kansas, and Texas Panhandle) statistically significant increasing trend. While the magnitude of the 99th percentile (Fig. 5c) and annual station maximum precipitation amount (Fig. 4c) trends are not large (>0.0–0.2 mm yr^{-1}), there are widespread statistically significant trends across the northern part of the study region, which is likely a continuation of the results found in the southern portion of the Missouri River basin (MORB) in Flanagan and Mahmood (2021). Although the MORB includes Kansas, the pattern continues into most of the central portion of the current SGP study area. Thus, this pattern of positive trends in DJF is likely driven by the same process, namely an increase in winter season air temperatures across the central GP driving an increase in atmospheric moisture. This increase in winter season atmospheric moisture can be explained by Clausius–Clapeyron theory, which notes that increase in temperature increases moisture holding capacity of air leading to higher extreme precipitation events (Kunkel et al. 2013). Previous research has shown that in the SGP winter (Mishra et al. 2012) subdaily precipitation extremes have a

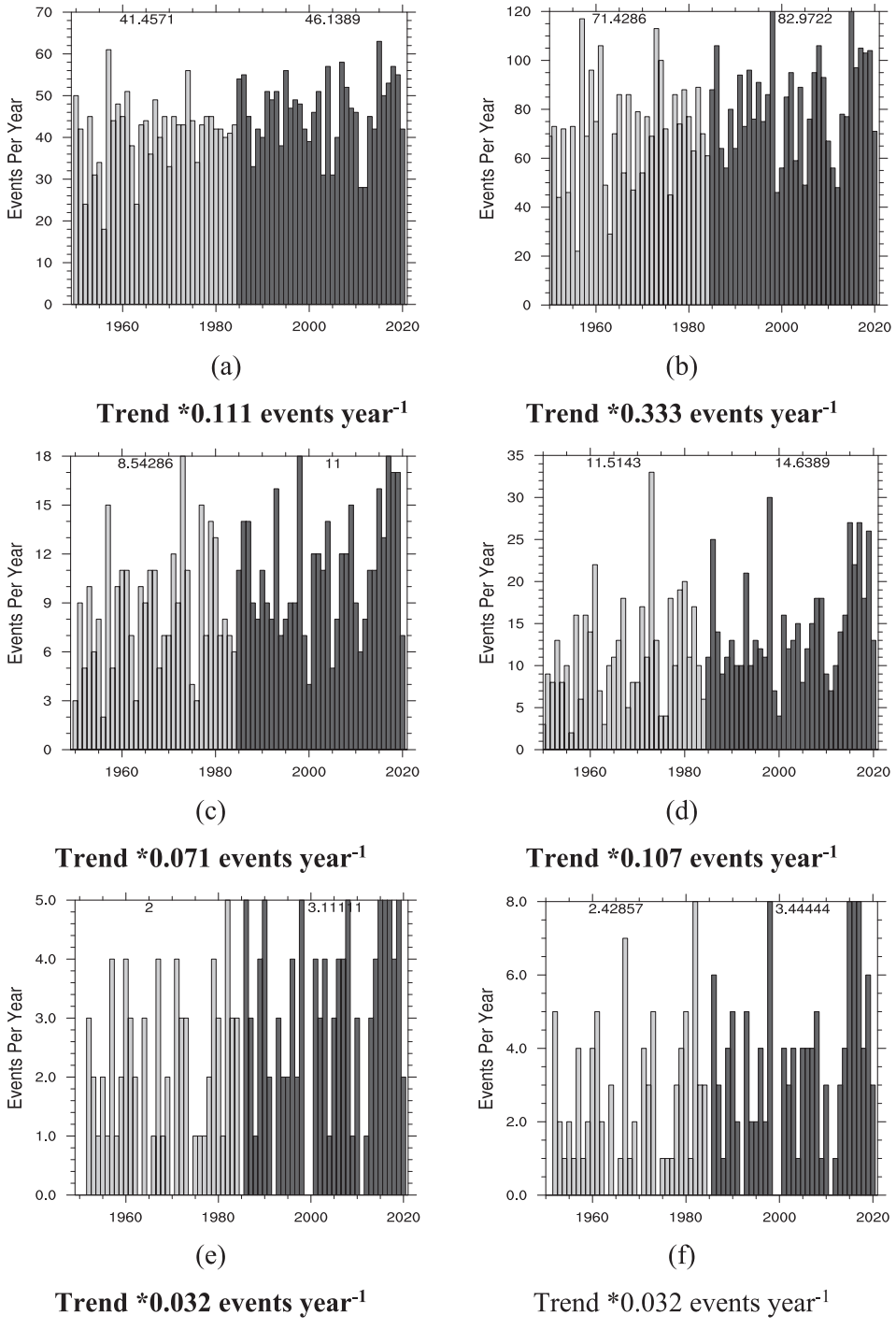

FIG. 6. Annual count of (left) unique (only one event counted per day, per year) precipitation events and (right) all-event precipitation events over (a),(b) 75; (c),(d) 125; and (e),(f) 175 mm across the study region. Light-gray bars are for events before 1985, and events after 1985 are shown with dark-gray bars. The numbers on the top of each plot represent the prior-to-1985 (left-hand side) and after-1985 (right-hand side) average number of events per year during that period. The trend for each plot is detailed below the figure label, with the asterisk showing that the specific trend is statistically significant at the 95% level using a Mann–Kendall test. Trends that are in boldface type indicate that the difference in means of the two periods is statistically significantly different using a *t* test with a *p* value of 0.05. The range of the *y* axis was allowed to change per plot so that the annual trend in the number of events could be detected visually.

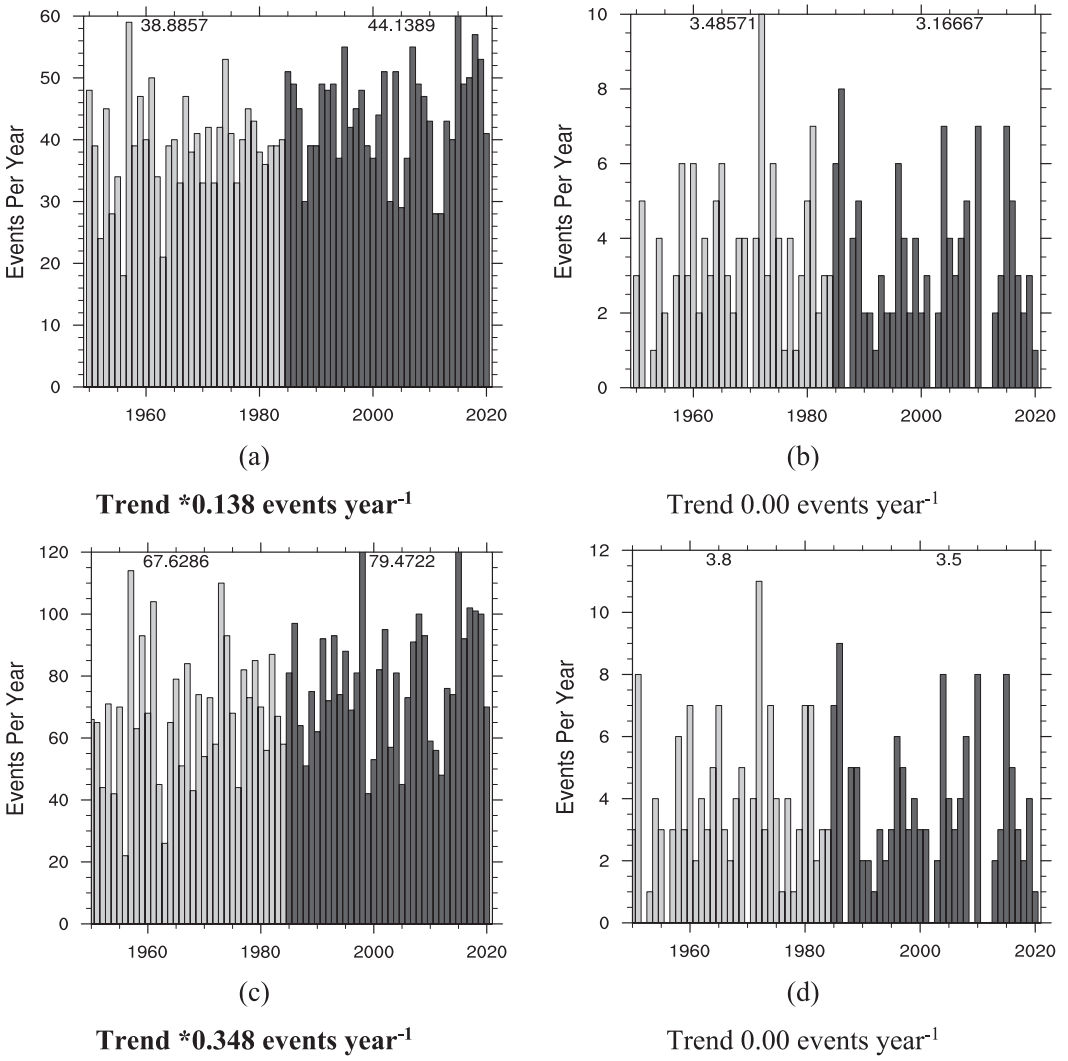

FIG. 7. As in Fig. 6, but of (top) unique (only one event counted per day, per year) precipitation events over 75 mm and (bottom) all-event precipitation events over 75 mm for (a),(c) eastern SGP and (b),(d) western SGP.

stronger link between temperature and the amount of precipitation received. Thus, it appears that the increasing winter extreme precipitation trend found in this work is likely linked to increased wintertime temperature over the central GP.

In the autumn (SON), few large (>0.4 mm yr^{-1}) statistically significant trends are analyzed in the annual station maximum (Fig. 4b) event analysis and 99th-percentile (Fig. 5b) trends (>0.2 mm yr^{-1}) along the eastern SGP Gulf Coast (eastern Texas and Louisiana). An analysis with TC events removed (not shown) did not noticeably alter the results of the 99th percentile or station maximum trends. TC event removal only slightly decreases the trends along the coast and modify statistical significance of trends of a few stations, thus negating TC events as the primary cause of the increased magnitudes of extreme precipitation. An increase in atmospheric moisture or moisture transport from the Gulf of Mexico is likely linked to the increase of SON extremes in the SGP and the Gulf of Mexico coastline. Further research is needed to investigate whether landfalling atmospheric rivers (Gimeno et al. 2016), anomalous Gulf of Mexico sea surface temperatures (SSTs), enhanced moisture transport into the GPLLJ from the Caribbean, and an increase in convective activity is linked to this coastal increase of extreme precipitation in the SGP. Outside of the statistically significant trends along the coastline, few statistically significant trends are seen scattered across the SGP region. Given the random scattering of these trends, it is difficult to come to any conclusions on the cause of these trends seen in the SGP.

In the spring (MAM) trend analyses (Figs. 4d and 5d), stations along the central and eastern Kansas and Oklahoma border are showing positive statistically significant trends. Given the location of these positive trends, several springtime features in the SGP could be impacting the trends. First, increases in the strength of the GPLLJ (Cook et al. 2008; Seager et al. 2014; Bukovsky et al. 2017) and or increased moisture flow from the Gulf of Mexico (e.g., Frei et al. 1998; Emori and Brown 2005; Santer et al. 2007; Trenberth 2011, 2012; Weaver et al. 2012; Molina and Allen 2020) could impact the region's

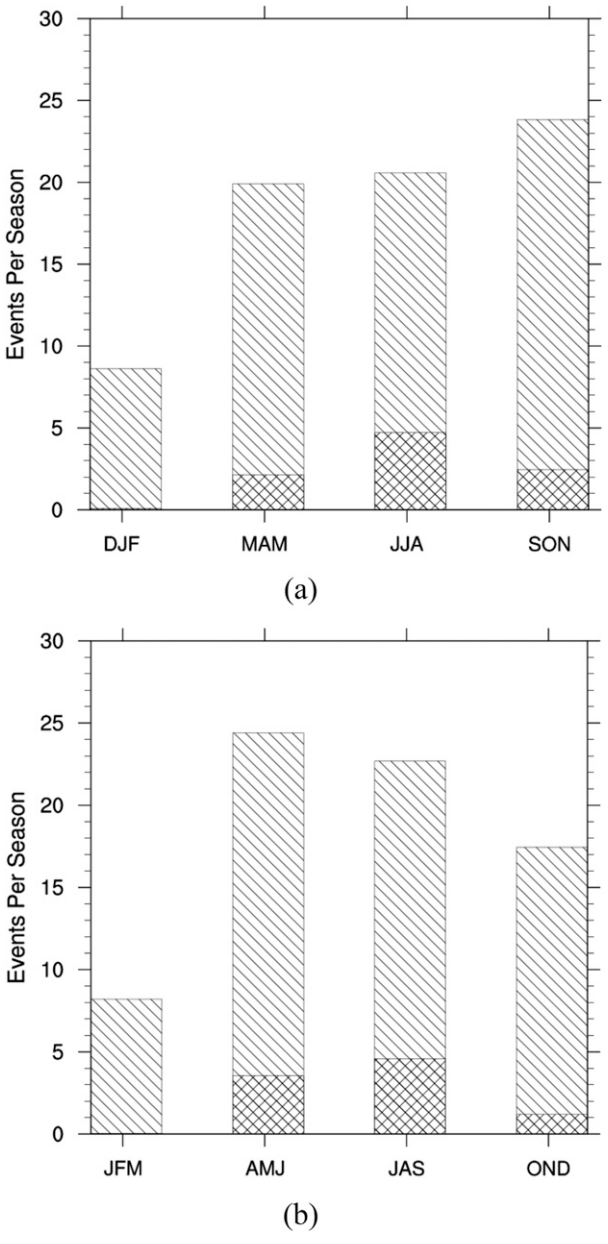

FIG. 8. All precipitation events over the all-station 99th percentile (73.7 mm) across four 3-month periods for all stations: east (hatched lines) and west (crosshatched lines) of 100°W. In (a), the typical 3-month (DJF, MAM, JJA, and SON) seasonal breakdown is used; in (b), the shifted 3-month (JFM, AMJ, JAS, and OND) seasonal breakdown is used. The counts of each 3-month period have been normalized by dividing through by the number of stations in each region (east and west of 100°W).

extreme precipitation magnitude. These positive trends could also be linked to shifts in the dryline, a prevalent feature of the SGP during the spring convective season. Changes in the frequency, strength of the moisture gradient, and or location of the dryline would dramatically impact convective precipitation during this season (Scaff et al. 2021).

In the summer (JJA), results continue to depict isolated and scattered statistically significant increasing trends across the SGP. Both the station annual maximum precipitation amount (Fig. 4e) and 99th-percentile (Fig. 5e) trends show scattered statistically significant trends across the region, except near the coastline, which lacks any statistically significant trends. A few isolated statistically significant trends can be seen in the southeastern portion of the SGP (eastern Texas), most statistically significant trends are in the northern SGP (Kansas and Colorado), which is the primary location of MCS activity within the SGP (Fritsch et al. 1986; Wang et al. 2013; Feng et al. 2016; Haberlie and Ashley 2019; Hu et al. 2021). As such, these spatially scattered central SGP statistically significant positive trends could be linked to an increase in frequency of intense MCS. In the western SGP, a few statistically significant increasing trends are depicted (as well as in SON), which could be connected to the North American monsoon (NAM; Higgins et al. 1997b, 1998). Because of the importance of the NAM to southwestern U.S. summer precipitation, extending as far east as the western extent of the study domain (western Texas and New Mexico), one can conjectured that JJA and SON precipitation extremes in this region could be connected to the moisture flow associated with NAM. However, given the lack of statistical significance in either the station maximum or 99th-percentile event analysis in the eastern SGP, our results do not support a conclusion of widespread change in extreme precipitation occurring during the summer. Moreover, several studies also suggest a weakening of the NAM precipitation linked to climate change induced warming (Pascale et al. 2017; Colorado-Ruiz et al. 2018). Because of the isolated and scattered nature of the trends seen in this analysis, further research is needed to make conclusions about the statistically significant positive trends found during the warm season.

The annual plots of station maximum (Fig. 4a) and 99th-percentile (Fig. 5a) trends agree with the results from the warm season (MAM, JJA, SON) seasonal analyses. All show isolated and spatially scattered statistically significant trends across the SGP, with SON (Figs. 4b and 5b) depicting more trends across the Gulf of Mexico coastline relative to MAM (Figs. 4d and 5d) and JJA (Figs. 4e and 5e), which are scattered across the inland area of the SGP. The annual plots show these trends as well, with a scattered spatial distribution of statistically significant trends across the SGP and a few are for stations along the Gulf of Mexico coast. However, the analyses of annual station maximum precipitation and 99th-percentile trends do not reflect the widespread central SGP (Kansas, Oklahoma, western Texas, and Colorado) results found in the DJF analyses (Figs. 4c and 5c). Given that extreme precipitation events in the DJF period are much less frequent it is unsurprising that the annual trends of the two measures of extreme precipitation do not reflect the apparent nature of DJF trends.

5. Conclusions

The goal of this study was to examine the fine-scale statistics of extreme precipitation within the SGP and identify station-scale

trends using station maximum and 99th-percentile definitions. While studies have investigated extreme precipitation within the SGP region (e.g., Mullens et al. 2013; Feng et al. 2016), or as part of a U.S.-wide regional breakdown (e.g., Kunkel et al. 1999; Min et al. 2011; Higgins and Kousky 2013; Easterling et al. 2017; Bartels et al. 2020; Kunkel et al. 2020; Davenport et al. 2021; Moustakis et al. 2021), few studies have included analyses at the station level within the SGP. While averaging across the entire region provides useful information, it loses a significant amount of detail, specifically within region variations such as the western, central, and eastern SGP. Furthermore, due to the bimodal (spring and autumn peaks) distribution of precipitation, a seasonal analysis of extreme precipitation is warranted to provide a complete picture of changes in extreme precipitation in the region.

The climatological spread of mean annual precipitation in the SGP ranges from over 1500 mm yr^{-1} in the eastern SGP to around 200–300 mm yr^{-1} in the western SGP (Fig. 1). In this context, a single day precipitation total on the magnitude of the all-station 99th percentile (73.7 mm) would constitute a small fraction of annual precipitation in the eastern SGP. On the other hand, it is nearly one-third of the annual precipitation in the western SGP. This type of precipitation event in the western SGP would lead to significant impacts, especially with the inability of hydrological infrastructure to handle this sudden influx of water (Osterkamp and Friedman 2000). In the eastern SGP, while these all-station 99th-percentile precipitation events may not have as large of an impact, beyond localized flash flooding, prolonged periods of multiple events, such as over a month or season, can lead to large-scale flooding. Such an event occurred in 2019, when numerous heavy precipitation episodes over a period of weeks in Kansas and Oklahoma led to a large flooding (Mesonet 2019; NWS 2019).

For this study, data from 108 USHCN stations spanning the 1950–2020 period in the SGP and surrounding states were analyzed. A 10% missing data threshold was used to remove stations with long stretches of missing data. Station maximum and 99th-percentile precipitation event trends were calculated along with counts of precipitation events crossing a threshold close to the all-station 99th percentile (75 mm) and in 50-mm increments above that (125 and 175 mm) to provide an in-depth analysis of temporal and spatial changes in extreme precipitation in the SGP. The climatological annual precipitation in the SGP notably decreases from east to west. This is reflected in our results for the station maximum precipitation event. The climatological frequency of extreme precipitation events also decreased from east to west across the SGP, even for the drier winter (DJF) season. Overall, our results show the following for the 1950–2020 period:

- Statistically significant trends for annual and JJA were isolated and spatially scattered.
- Statistically significant trends for MAM showed a distinct increasing trend along the Kansas and Oklahoma border.
- Statistically significant trends for DJF suggest widespread increasing trends across Oklahoma, Kansas, and the Texas Panhandle.
- Statistically significant trends for SGP Gulf of Mexico coast in SON were found to be unrelated to TC events.
- The eastern SGP shows many stations with large (>0.2 mm yr^{-1}) statistically significant positive trends, while in the western SGP a few stations were found with statistically significant increasing trends. However, in terms of percentage the western SGP has more statistically significant stations than the eastern SGP.
- MAM, JJA, and SON show statistically significant and scattered large (>0.2 mm yr^{-1}) positive trends in the inland part of the SGP. The findings are likely associated with increased atmospheric moisture content related warming of the atmosphere and or increased SST in the Gulf of Mexico (leading to higher evaporation and moisture flow to the SGP from the Gulf).
- Comparison of the periods before and after 1984 suggests statistically significant increases in the all-event with ≥75-, ≥125-, and ≥175-mm threshold.
- Comparison of the periods before and after 1984 shows small increases in unique event counts for the ≥75-, ≥125-, and ≥175-mm thresholds.
- Comparison of the event counts suggests that, while increases occurred for both unique and all-event counts, the all-event counts indicate larger and more consistent increases within the >75-mm-magnitude analysis. This indicates that the spatial extent of these extreme events is increasing.

These results largely agree with previous studies investigating extreme precipitation in the SGP (e.g., Kunkel et al. 1999; Min et al. 2011; Higgins and Kousky 2013; Mullens et al. 2013; Feng et al. 2016; Easterling et al. 2017; Bartels et al. 2020; Kunkel et al. 2020; Davenport et al. 2021; Moustakis et al. 2021), which show an increase in the right tail of the precipitation distribution, meaning an increase in the magnitude of the heaviest precipitation events. Our results showed this finding well, with the annual station maximum and 99th-percentile events becoming more intense since 1950. This is more reflected within the non–statistically significant results, while the statistically significant results depict isolated and scattered increases during most of the year. Based on the agreement of results between this and previous studies, it is likely that a regionwide shift in extreme precipitation is occurring. It is particularly noticeable in DJF and in the northern areas of this specific SGP domain.

The event counts produced a different result. They suggest a larger trend in the spatial extent of extreme precipitation events (those ≥75 mm), observed in both the western and eastern SGP. Thus, while the magnitude of these events does not appear to be changing in the western SGP, the spatial extent is increasing. An increase in the number of stations impacted by extreme precipitation events in the western SGP could mean challenges for the region, as more widespread extreme precipitation would cause more widespread erosion (Joyce et al. 2001; Thornes 2007; Papanastasis 2009). More specific land management is necessary with an increase in erosion within this region to maintain adequate grazing land for the livestock industry, which is prevalent in the western SGP.

In this study, liquid equivalent precipitation is considered from the USHCN station network. Thus, frozen precipitation is not specifically addressed. Since the results suggest many

inland stations observed statistically significant increasing trends during the winter season, an analysis of frozen precipitation with respect to winter extremes is necessary to identify the direct cause of these widespread increasing trends. Further studies are also necessary to investigate the increasing station coverage of extreme precipitation events within this region. The spatial extent of extreme precipitation has direct impacts on flash flooding, and downstream flooding. In the context of the results from Flanagan and Mahmood (2021) and this study, further research investigating the GPLLJ in conjunction with GP extreme precipitation is necessary. One caveat to note is the choice of temporal period over which the trends were calculated. This study analyzed trends over the 1950–2020 period (due to the availability of reliable data); a different choice of period would likely produce different results depending on the period chosen. A short analysis was completed to address this notion. It was found that as the starting time comes closer to the present (i.e., starting period for analysis 2000, vs 1990, 1980, 1970, etc.) the positive extreme precipitation magnitude trends became larger and more widespread within the SGP. Thus, choice of start and end dates for such an analysis within the SGP should be carefully selected, because the result can be biased if shorter or more recent dates are chosen.

Acknowledgments. The authors thank three anonymous reviewers and the editor for their valuable comments and suggestions, which helped to improve this paper.

Data availability statement. Datasets analyzed within the current study are available in the NCEI data repository (https://www.ncei.noaa.gov/pub/data/ghcn/daily/).

REFERENCES

Adhikari, A., and A. J. Hansen, 2019: Climate and water balance change among public, private, and tribal lands within greater wildland ecosystems across north central USA. *Climatic Change*, **152**, 551–567, https://doi.org/10.1007/s10584-018-2351-7.

——, ——, and I. Rangwala, 2019: Ecological water stress under projected climate change across hydroclimate gradients in the north-central United States. *J. Appl. Meteor. Climatol.*, **58**, 2103–2114, https://doi.org/10.1175/JAMC-D-18-0149.1.

Bartels, R. J., A. W. Black, and B. D. Keim, 2020: Trends in precipitation days in the United States. *Int. J. Climatol.*, **40**, 1038–1048, https://doi.org/10.1002/joc.6254.

Berg, L. K., L. D. Riihimaki, Y. Qian, H. Yan, and M. Huang, 2015: The low-level jet over the southern Great Plains determined from observations and reanalyses and its impact on moisture transport. *J. Climate*, **28**, 6682–6706, https://doi.org/10.1175/JCLI-D-14-00719.1.

Borchert, J. R., 1950: The climate of the central North American grassland. *Ann. Assoc. Amer. Geogr.*, **40** (1), 1–39, https://doi.org/10.1080/00045605009352020.

Bukovsky, M. S., R. R. McCrary, A. Seth, and L. O. Mearns, 2017: A mechanistically credible, poleward shift in warm-season precipitation projected for the U.S. southern Great Plains? *J. Climate*, **30**, 8275–8298, https://doi.org/10.1175/JCLI-D-16-0316.1.

Christian, J., K. Christian, and J. B. Basara, 2015: Drought and pluvial dipole events within the Great Plains of the United States. *J. Appl. Meteor. Climatol.*, **54**, 1886–1898, https://doi.org/10.1175/JAMC-D-15-0002.1.

Colorado-Ruiz, G., T. Cavazos, J. A. Salinas, P. De Grau, and R. Ayala, 2018: Climate change projections from Coupled Model Intercomparison Project phase 5 multi-model weighted ensembles for Mexico, the North American monsoon, and the mid-summer drought region. *Int. J. Climatol.*, **38**, 5699–5716, https://doi.org/10.1002/joc.5773.

Cook, K. H., E. K. Vizy, Z. S. Launer, and C. M. Patricola, 2008: Springtime intensification of the Great Plains low-level jet and Midwest precipitation in GCM simulations of the twenty-first century. *J. Climate*, **21**, 6321–6340, https://doi.org/10.1175/2008JCLI2355.1.

Davenport, F. V., M. Burke, and N. S. Diffenbaugh, 2021: Contribution of historical precipitation change to US flood damages. *Proc. Natl. Acad. Sci. USA*, **118**, e2017524118–, https://doi.org/10.1073/pnas.2017524118.

Deng, Y., and T. Jiang, 2011: Intraseasonal modulation of the North Pacific storm track by tropical convection in boreal winter. *J. Climate*, **24**, 1122–1137, https://doi.org/10.1175/2010JCLI3676.1.

Doswell, C. A., H. E. Brooks, and R. A. Maddox, 1996: Flash flood forecasting: An ingredients-based methodology. *Wea. Forecasting*, **11**, 560–581, https://doi.org/10.1175/1520-0434(1996)011<0560:FFFAIB>2.0.CO;2.

Doyle, T. W., 2009: Hurricane frequency and landfall distribution for coastal wetlands of the Gulf Coast, USA. *Wetlands*, **29**, 35–43, https://doi.org/10.1672/08-36.1.

Durre, I., M. J. Menne, B. E. Gleason, T. G. Houston, and R. S. Vose, 2010: Robust automated quality control of daily surface observations. *J. Appl. Meteor. Climatol.*, **49**, 1615–1633, https://doi.org/10.1175/2010JAMC2375.1.

Easterling, D. R., and Coauthors, 2017: Precipitation change in the United States. *Climate Science Special Report: Fourth National Climate Assessment*, Vol. I, D. J. Wuebbles et al., Eds., U.S. Global Change Research Program, 207–230, https://doi.org/10.7930/J0H993CC.

Emori, S., and S. J. Brown, 2005: Dynamic and thermodynamic changes in mean and extreme precipitation under changed climate. *Geophys. Res. Lett.*, **32**, L17706, https://doi.org/10.1029/2005GL023272.

Feng, Z., L. R. Leung, S. Hagos, R. A. Houze, C. D. Burleyson, and K. Balaguru, 2016: More frequent intense and long-lived storms dominate the springtime trend in central U.S. rainfall. *Nat. Commun.*, **7**, 13429, https://doi.org/10.1038/ncomms13429.

Flanagan, P. X., and R. Mahmood, 2021: Spatiotemporal analysis of extreme precipitation in the Missouri River basin from 1950–2019. *J. Appl. Meteor. Climatol.*, **60**, 811–827, https://doi.org/10.1175/JAMC-D-20-0212.1.

——, J. B. Basara, and X. Xiao, 2017: Long-term analysis of the asynchronicity between temperature and precipitation maxima in the United States Great Plains. *Int. J. Climatol.*, **37**, 3919–3933, https://doi.org/10.1002/joc.4966.

——, ——, J. C. Furtado, and X. Xiao, 2018: Primary atmospheric drivers of pluvial years in the United States Great Plains. *J. Hydrometeor.*, **19**, 643–658, https://doi.org/10.1175/JHM-D-17-0148.1.

——, and Coauthors, 2020: A hydrometeorological assessment of the historic 2019 flood of Nebraska, Iowa, and South Dakota. *Bull. Amer. Meteor. Soc.*, **101**, E817–E829, https://doi.org/10.1175/BAMS-D-19-0101.1.

Frei, C., C. Schär, D. Lüthi, and H. C. Davies, 1998: Heavy precipitation processes in a warmer climate. *Geophys. Res. Lett.*, **25**, 1431–1434, https://doi.org/10.1029/98GL51099.

Fritsch, J. M., R. J. Kane, and C. R. Chelius, 1986: The contribution of mesoscale convective weather systems to the warm-season precipitation in the United States. *J. Climate Appl. Meteor. Climatol.*, **25**, 1333–1345, https://doi.org/10.1175/1520-0450(1986)025<1333:TCOMCW>2.0.CO;2.

Ghimire, R., B. Ghimire, A. O. Mesbah, O. J. Idowu, M. K. O'Neill, S. V. Angadi, and M. K. Shukla, 2018: Current status, opportunities and challenges of cover cropping for sustainable dryland farming in the southern Great Plains. *J. Crop Improv.*, **32**, 579–598, https://doi.org/10.1080/15427528.2018.1471432.

Gimeno, L., and Coauthors, 2016: Major mechanisms of atmospheric moisture transport and their role in extreme precipitation events. *Annu. Rev. Environ. Resour.*, **41**, 117–141, https://doi.org/10.1146/annurev-environ-110615-085558.

Grise, K. M., S.-W. Son, and J. R. Gyakum, 2013: Intraseasonal and interannual variability in North American storm tracks and its relationship to equatorial Pacific variability. *Mon. Wea. Rev.*, **141**, 3610–3625, https://doi.org/10.1175/MWR-D-12-00322.1.

Haberlie, A. M., and W. S. Ashley, 2019: A radar-based climatology of mesoscale convective systems in the United States. *J. Climate*, **32**, 1591–1606, https://doi.org/10.1175/JCLI-D-18-0559.1.

Hayhoe, K., and Coauthors, 2018: Our changing climate. *Impacts, Risks, and Adaptation in the United States: Fourth National Climate Assessment*, Vol. II, D. R. Reidmiller et al., Eds., U.S. Global Change Research Program, 72–144, https://doi.org/10.7930/NCA4.2018.CH2.

Helfand, H. M., and S. D. Schubert, 1995: Climatology of the simulated Great Plains low-level jet and its contribution to the continental moisture budget of the United States. *J. Climate*, **8**, 784–806, https://doi.org/10.1175/1520-0442(1995)008<0784:COTSGP>2.0.CO;2.

Higgins, R. W., and V. E. Kousky, 2013: Changes in observed daily precipitation over the United States between 1950–79 and 1980–2009. *J. Hydrometeor.*, **14**, 105–121, https://doi.org/10.1175/JHM-D-12-062.1.

——, Y. Yao, E. S. Yarosh, J. E. Janowiak, and K. C. Mo, 1997a: Influence of the Great Plains low-level jet on summer-time precipitation and moisture transport over the central United States. *J. Climate*, **10**, 481–507, https://doi.org/10.1175/1520-0442(1997)010<0481:IOTGPL>2.0.CO;2.

——, ——, and X. L. Wang, 1997b: Influence of the North American monsoon system on the U.S. summer precipitation regime. *J. Climate*, **10**, 2600–2622, https://doi.org/10.1175/1520-0442(1997)010<2600:IOTNAM>2.0.CO;2.

——, K. C. Mo, and Y. Yao, 1998: Interannual variability of the U.S. summer precipitation regime with emphasis on the southwestern monsoon. *J. Climate*, **11**, 2582–2606, https://doi.org/10.1175/1520-0442(1998)011<2582:IVOTUS>2.0.CO;2.

Hoch, J., and P. Markowski, 2005: A climatology of springtime dryline position in the U.S. Great Plains region. *J. Climate*, **18**, 2132–2137, https://doi.org/10.1175/JCLI3392.1.

Howarth, M. E., D. C. Thorncroft, and L. F. Bosart, 2019: Changes in extreme precipitation in the northeast United States: 1979–2014. *J. Hydrometeor.*, **20**, 673–689, https://doi.org/10.1175/JHM-D-18-0155.1.

Hu, H., Z. Feng, and L.-Y. R. Leung, 2021: Linking flood frequency with mesoscale convective systems in the US. *Geophys. Res. Lett.*, **48**, e2021GL092546, https://doi.org/10.1029/2021GL092546

Illston, B. G., J. B. Basara, and K. C. Crawford, 2004: Seasonal to interannual variations of soil moisture measured in Oklahoma. *Int. J. Climatol.*, **24**, 1883–1896, https://doi.org/10.1002/joc.1077.

Janssen, E., D. J. Wuebbles, K. E. Kunkel, S. C. Olsen, and A. Goodman, 2014: Observational- and model-based trends and projections of extreme precipitation over the contiguous United States. *Earth's Future*, **2**, 99–113, https://doi.org/10.1002/2013EF000185.

Joyce, L. A., D. Ojima, G. A. Seiclstad, R. Harriss, and J. Backell, 2001: Potential consequences of climate variability and change for the Great Plains. *The Potential Consequences of Climate Variability and Change*, Cambridge University Press, 191–217.

Kendall, M. G., 1975: *Rank Correlation Methods*. 4th ed. Charles Griffin, 202 pp.

Kunkel, K. E., K. Andsager, and D. R. Easterling, 1999: Long-term trends in extreme precipitation events over the conterminous United States and Canada. *J. Climate*, **12**, 2515–2527, https://doi.org/10.1175/1520-0442(1999)012<2515:LTTIEP>2.0.CO;2.

——, T. R. Karl, D. R. Easterling, K. Redmond, J. Young, X. Yin, and P. Hennon, 2013: Probable maximum precipitation and climate change. *Geophys. Res. Lett.*, **40**, 1402–1408, https://doi.org/10.1002/grl.50334.

——, ——, M. F. Squires, X. Yin, S. T. Stegall, and D. R. Easterling, 2020: Precipitation extremes: Trends and relationships with average precipitation and precipitable water in the contiguous United States. *J. Appl. Meteor. Climatol.*, **59**, 125–142, https://doi.org/10.1175/JAMC-D-19-0185.1.

Liu, L., and B. Basso, 2020: Impacts of climate variability and adaptation strategies on crop yields and soil organic carbon in the US Midwest. *PLOS ONE*, **15**, e0225433, https://doi.org/10.1371/journal.pone.0225433.

Livneh, B., and M. P. Hoerling, 2016: The physics of drought in the U.S. central Great Plains. *J. Climate*, **29**, 6783–6804, https://doi.org/10.1175/JCLI-D-15-0697.1.

Lyons, S. W., 2004: U.S. tropical cyclone landfall variability: 1950–2002. *Wea. Forecasting*, **19**, 473–480, https://doi.org/10.1175/1520-0434(2004)019<0473:UTCLV>2.0.CO;2.

Mäkinen, H., and Coauthors, 2018: Sensitivity of European wheat to extreme weather. *Field Crops Res.*, **222**, 209–217, https://doi.org/10.1016/j.fcr.2017.11.008.

Malinowski, D. P., W. E. Pinchak, B. A. Kramp, H. Zuo, and T. J. Butler, 2007: Supplemental irrigation and fall dormancy effects on alfalfa productivity in a semiarid, subtropical climate with a bimodal precipitation pattern. *Agron. J.*, **99**, 621–629, https://doi.org/10.2134/agronj2006.0056.

Mallakpour, I., and G. Villarini, 2015: The changing nature of flooding across the central United States. *Nat. Climate Change*, **5**, 250–254, https://doi.org/10.1038/nclimate2516.

Mann, H. B., 1945: Nonparametric test against trend. *Econometrica*, **13**, 245–259, https://doi.org/10.2307/1907187.

Menne, M. J., and Coauthors, 2012: Global historical climatology network–Daily (GHCN-Daily), version 3. USHCN Stations, NOAA National Climatic Data Center, accessed 14 September 2021, https://doi.org/10.7289/V5D21VHZ.

Mesonet, 2019: May weather brings disaster to Oklahoma. Accessed 17 February 2022, https://www.mesonet.org/news/may-weather-brings-disaster-to-oklahoma.

Michaud, J. D., K. K. Hirschboeck, and M. Winchell, 2001: Regional variations in small-basin floods in the United States. *Water Resour. Res.*, **37**, 1405–1416, https://doi.org/10.1029/2000WR900283.

Min, S.-K., X. Zhang, F. W. Zwiers, and G. C. Hegerl, 2011: Human contribution to more-intense precipitation extremes. *Nature*, **470**, 378–381, https://doi.org/10.1038/nature09763.

Mishra, V., J. M. Wallace, and D. P. Lettenmaier, 2012: Relationship between hourly extreme precipitation and local air temperature in the United States. *Geophys. Res. Lett.*, **39**, L16403, https://doi.org/10.1029/2012GL052790.

Mitchell, T., and D. M. Schultz, 2020: A synoptic climatology of spring dryline convection in the southern Great Plains. *Wea. Forecasting*, **35**, 1561–1582, https://doi.org/10.1175/WAF-D-19-0160.1.

Mock, C. J., 1996: Climatic controls and spatial variations of precipitation in the western United States. *J. Climate*, **9**, 1111–1125, https://doi.org/10.1175/1520-0442(1996)009<1111:CCASVO>2.0.CO;2.

Molina, M. J., and J. T. Allen, 2020: Regionally-stratified tornadoes: Moisture source physical reasoning and climate trends. *Wea. Climate Extremes*, **28**, 100244, https://doi.org/10.1016/j.wace.2020.100244.

Montgomery, D. R., 2007: Soil erosion and agricultural sustainability. *Proc. Natl. Acad. Sci. USA*, **104**, 13 268–13 272, https://doi.org/10.1073/pnas.0611508104.

Moustakis, Y., S. M. Papalexiou, C. J. Onof, and A. Paschalis, 2021: Seasonality, intensity, and duration of rainfall extremes change in a warmer climate. *Earth's Future*, **9**, e2020EF001824, https://doi.org/10.1029/2020EF001824.

Mullens, E. D., 2021: Meteorological cause and characteristics of widespread heavy precipitation in the Texas Gulf watershed 2003–2018. *Int. J. Climatol.*, **41**, 3743–3760, https://doi.org/10.1002/joc.7046.

——, and R. A. McPherson, 2019: Quantitative scenarios for future hydrologic extremes in the U.S. southern Great Plains. *Int. J. Climatol.*, **39**, 2659–2676, https://doi.org/10.1002/joc.5979.

——, M. Shafer, and J. Hocker, 2013: Trends in heavy precipitation in the southern USA. *Weather*, **68**, 311–316, https://doi.org/10.1002/wea.2113.

Neild, R. E., 1982: Temperature and rainfall influences on the phenology and yield of grain sorghum and maize: A comparison. *Agric. Meteor.*, **27**, 79–88, https://doi.org/10.1016/0002-1571(82)90022-X.

NWS, 2019: May 20th–28th significant flooding. NOAA, accessed 17 February 2022, https://www.weather.gov/ict/event_20190520.

Osterkamp, W. R., and J. M. Friedman, 2000: The disparity between extreme rainfall events and rare floods—With emphasis on the semiarid American West. *Hydrol. Processes*, **14**, 2817–2829, https://doi.org/10.1002/1099-1085(200011/12)14:16/17<2817::AID-HYP121>3.0.CO;2-B.

Papanastasis, V. P., 2009: Restoration of degraded grazing lands through grazing management: Can it work? *Restor. Ecol.*, **17**, 441–445, https://doi.org/10.1111/j.1526-100X.2009.00567.x.

Pascale, S., W. R. Boos, S. Bordoni, T. L. Delworth, S. B. Kapnick, H. Murakami, G. A. Vecchi, and W. Zhang, 2017: Weakening of the North American monsoon with global warming. *Nat. Climate Change*, **7**, 806–812, https://doi.org/10.1038/nclimate3412.

Patrignani, A., R. P. Lollato, T. E. Ochsner, C. B. Godsey, and J. T. Edwards, 2014: Yield gap and production gap of rainfed winter wheat in the southern Great Plains. *Agron. J.*, **106**, 1329–1339, https://doi.org/10.2134/agronj14.0011.

Pimentel, D., and Coauthors, 1987: World agriculture and soil erosion. *BioScience*, **37**, 277–283, https://doi.org/10.2307/1310591.

Qiao, L., C. B. Zou, C. F. Gaitán, Y. Hong, and R. A. McPherson, 2017: Analysis of precipitation projections over the climate gradient of the Arkansas Red River basin. *J. Appl. Meteor. Climatol.*, **56**, 1325–1336, https://doi.org/10.1175/JAMC-D-16-0201.1.

Rosenberg, N. J., and S. J. Smith, 2009: A sustainable biomass industry for the North American Great Plains. *Environ. Sustainability*, **1**, 121–132, https://doi.org/10.1016/j.cosust.2009.09.003.

Ruiz-Barradas, A., and S. Nigam, 2005: Warm-season precipitation variability over the U.S. Great Plains in observations, NCEP and ERA-40 reanalyses, and NCAR and NASA atmospheric model simulations. *J. Climate*, **18**, 1808–1830, https://doi.org/10.1175/JCLI3343.1.

——, and ——, 2006: IPCC's twentieth-century climate simulations: Varied representations of North American hydroclimate variability. *J. Climate*, **19**, 4041–4058, https://doi.org/10.1175/JCLI3809.1.

——, and ——, 2010: Great Plains precipitation and its SST links in twentieth century climate simulations, and twenty-first- and twenty-second-century climate projections. *J. Climate*, **23**, 6409–6429, https://doi.org/10.1175/2010JCLI3173.1.

Santer, B. D., and Coauthors, 2007: Identification of human-induced changes in atmospheric moisture content. *Proc. Natl. Acad. Sci. USA*, **104**, 15 248–15 253, https://doi.org/10.1073/pnas.0702872104.

Scaff, L., and Coauthors, 2021: Dryline characteristics in North America's historical and future climates. *Climate Dyn.*, **57**, 2171–2188, https://doi.org/10.1007/s00382-021-05800-1.

Schumacher, R. S., and R. H. Johnson, 2005: Organization and environmental properties of extreme-rain-producing mesoscale convective systems. *Mon. Wea. Rev.*, **133**, 961–976, https://doi.org/10.1175/MWR2899.1.

Seager, R., and Coauthors, 2014: Dynamical and thermodynamical causes of large-scale changes in the hydrological cycle over North America in response to global warming. *J. Climate*, **27**, 7921–7948, https://doi.org/10.1175/JCLI-D-14-00153.1.

——, N. Lis, J. Feldman, M. Ting, A. P. Williams, J. Nakamura, H. Liu, and N. Henderson, 2018: Whither the 100th meridian? The once and future physical and human geography of America's arid–humid divide. Part I: The story so far. *Earth Interact.*, **22**, https://doi.org/10.1175/EI-D-17-0011.1.

Sharpley, A. N., S. J. Smith, and J. W. Naney, 1987: Environmental impact of agricultural nitrogen and phosphorus use. *J. Agric. Food Chem.*, **35**, 812–817, https://doi.org/10.1021/jf00077a043.

Simon Wang, S.-Y., W.-R. Huang, H.-H. Hsu, and R. R. Gillies, 2015: Role of the strengthened El Niño teleconnection in the May 2015 floods over the southern Great Plains. *Geophys. Res. Lett.*, **42**, 8140–8146, https://doi.org/10.1002/2015GL065211.

Song, J., K. Liao, R. L. Coulter, and B. M. Lesht, 2005: Climatology of the low-level jet at the southern Great Plains atmospheric boundary layer experiment site. *J. Appl. Meteor.*, **44**, 1593–1606, https://doi.org/10.1175/JAM2294.1.

Thornes, J. B., 2007: Modelling soil erosion by grazing: Recent developments and new approaches. *Geogr. Res.*, **45**, 13–26, https://doi.org/10.1111/j.1745-5871.2007.00426.x.

Ting, M., and H. Wang, 1997: Summertime U.S. precipitation variability and its relation to Pacific sea surface temperature. *J. Climate*, **10**, 1853–1873, https://doi.org/10.1175/1520-0442(1997)010<1853:SUSPVA>2.0.CO;2.

Tollerud, H., J. Brown, T. Loveland, R. Mahmood, and N. Bliss, 2018: Drought and land-cover conditions in the Great Plains. *Earth Interact.*, **22**, https://doi.org/10.1175/EI-D-17-0025.1.

Trenberth, K. E., 2011: Changes in precipitation with climate change. *Climate Res.*, **47**, 123–138, https://doi.org/10.3354/cr00953.

——, 2012: Framing the way to relate climate extremes to climate change. *Climatic Change*, **115**, 283–290, https://doi.org/10.1007/s10584-012-0441-5.

Urban, D. W., M. J. Roberts, W. Schlenker, and D. B. Lobell, 2015: The effects of extremely wet planting conditions on

maize and soybean yields. *Climatic Change*, **130**, 247–260, https://doi.org/10.1007/s10584-015-1362-x.

Wang, S.-Y., R. E. Davies, and R. R. Gillies, 2013: Identification of extreme precipitation threat across midlatitude regions based on short-wave circulations. *J. Geophys. Res. Atmos.*, **118**, 11 059–11 074, https://doi.org/10.1002/jgrd.50841.

Weaver, S. J., and S. Nigam, 2008: Variability of the Great Plains low-level jet: Large-scale circulation context and hydroclimate impacts. *J. Climate*, **21**, 1532–1551, https://doi.org/10.1175/2007JCLI1586.1.

——, S. Baxter, and A. Kumar, 2012: Climatic role of North American low-level jets on U.S. regional tornado activity. *J. Climate*, **25**, 6666–6683, https://doi.org/10.1175/JCLI-D-11-00568.1.

Westra, S., and Coauthors, 2014: Future changes to the intensity and frequency of short-duration extreme rainfall. *Rev. Geophys.*, **52**, 522–555, https://doi.org/10.1002/2014RG000464.

Wilcox, R. R., and J. Muska, 1999: Tests of hypotheses about regression parameters when using a robust estimator. *Commun. Stat. Theory Methods*, **28**, 2201–2212, https://doi.org/10.1080/03610929908832415.

Wugofski, S., 2019: Synoptic and mesoscale analysis of the 2015 southern Great Plains flash pluvial. M.S. thesis, School of Meteorology, University of Oklahoma, 122 pp.